IET Generation, Transmission & Distribution

Research Article

IET Journals
The Institution of Engineering and Technology

Modelling, simulation, and verification for detailed short-circuit analysis of a 1 × 25 kV railway traction system

ISSN 1751-8687
Received on 11th April 2015
Revised on 12th October 2015
Accepted on 27th October 2015
doi: 10.1049/iet-gtd.2015.0501
www.ietdl.org

Tsai-Hsiang Chen, Rih-Neng Liao ✉

Department of Electrical Engineering, National Taiwan University of Science and Technology, 43, Keelung Road, Section 4, Taipei 10607, Taiwan
✉ *E-mail: d9807104@gmail.com*

Abstract: This study presents a modelling and simulation method for the analysis of short-circuits in 1 × 25 kV railway traction systems (RTSs). First, the authors developed models of major components and a full-scale model of a RTS. The component models developed in this study include a specific Le Blanc traction transformer and an overhead catenary system. The models are represented using corresponding coupling-free equivalent circuits to facilitate implementation using software packages MATLAB®/Simulink®. The short-circuit fault simulation of a RTS was conducted on a personal computer operating with MS Windows 7®. Field testing data was used to verify the simulation results. The modelling and simulation technology developed in this study provide a valuable reference for power engineers involved in the planning, design, and operation of a railway traction network.

1 Introduction

The electric locomotive is a strong contender for the title of the most efficient and economical motive power for high-density transportation systems. In the final decades of the twentieth century, the steam railway system in Taiwan was converted to electricity. In late 2014, the railway electrification system from Hualien to Taitung was completed, thereby largely overcoming the traffic problems in Eastern Taiwan. Power to the railway is supplied by nearby traction substations fed from a three-phase 69-kV high-voltage grid of the Taiwan Power Company (TPC).

Single-phase 1 × 25-kV and autotransformer-fed 2 × 25-kV traction systems are commonly used in modern railway electrification system, including high-speed railways [1, 2]. The short-circuit fault current in an autotransformer-fed 2 × 25-kV traction system tends to exceed that in a 1 × 25-kV traction system, and fault locating is more complicated [3]. In 1 × 25-kV traction systems, the large single-phase non-linear traction loads supplied by three-phase power systems also tend to cause the voltage unbalance, voltage fluctuation, harmonic pollution, and problems associated with a poor power quality [4, 5].

Short-circuit analysis is critical in determining the rating of power equipment and the implementation of protection devices, as well as can also be used to check the voltage profile of a network, particularly the busses near a fault. Particular attention must be paid to an accurate modelling of the traction transformers, autotransformers as well as self and mutual impedances of the AC railway overhead contact line systems. In short-circuits analysis, the impedance of system components and the configuration of the railway traction system (RTS) are the main factors determining the short-circuit current. This paper examines a single-phase 1 × 25 kV RTS in which the key factors determining the fault current are as follows:

(i) The short-circuit capacity (SCC) at the busbar on the primary side of the traction transformer; that is, the source transformer.
(ii) The winding connections (Le Blanc) and impedance of transformers in traction substations.
(iii) The self and mutual impedances of overhead contact systems (including overhead messenger wire, overhead trolley contact wire, and return feeders) as well as the rails.

Estimating disturbances resulting from the various types of short-circuit faults require comprehensive data collection with regards to all major components and the overall RTS, while the operating conditions of the RTS (both normal and abnormal) must also be considered. In the technical literature, several studies have been performed on: (i) traction system design, components modelling, and calculation methods [6–11] and (ii) critical and short-circuit conditions [12–15]. A detailed short-circuit modelling of a RTS can be derived and implemented in the time and frequency domains. In general, a frequency domain simulation is considered a feasible solution for the steady-state analysis, and it is typically used for both, system design and harmonic studies. The time domain simulation is generally used for transient analysis, in which information on the waveform characteristics and time evolution are required. In [16, 17], a time-domain model of a complete 2 × 25-kV high-speed railway system was proposed using the MATLAB®/Simulink® Power System Blockset (PSB) tool, where short-circuit analyses were performed. To reduce the complexity of the simulations, simplified models were proposed in [14, 18, 19]. In [14], only three major lines (overhead contact wire, return feeder, and rail) in the overhead catenary system (OCS) are considered. In [18, 19], simplified models are suggested to reduce the number of phases of the system by grouping the conductors. These models are suitable for applications where details for each individual line are not examined. Moreover, some components are mathematically represented by algebraic equations rather than by physical elements (R, L, or C); thus, these component models cannot be directly applied to commercial circuit simulation programs. Although, several component models have been developed in existing commercial software packages, including (i) a specific traction transformer and (ii) a detailed overhead contact lines system (existing in MATLAB®/Simulink® PSB tool; however, their functions are insufficient for detailed analysis such as asymmetrical structure simulation). Therefore, to ensure accurate simulation and easy implementation of RTSs, more detailed models of RTSs need to be developed.

In this study, we developed a system of modelling and simulated for the analysis of short-circuits in a full-scale 1 × 25 kV RTS, including all major components. All models are represented using their corresponding coupling-free equivalent circuits to facilitate implementation within in-house or commercial software packages, such as the Electromagnetic Transients Program, the Personal Computer Simulation Program with Integrated Circuit Emphasis, MATLAB®/Simulink®, or self-developed program for short-circuits analysis. We then applied the models to the development of a

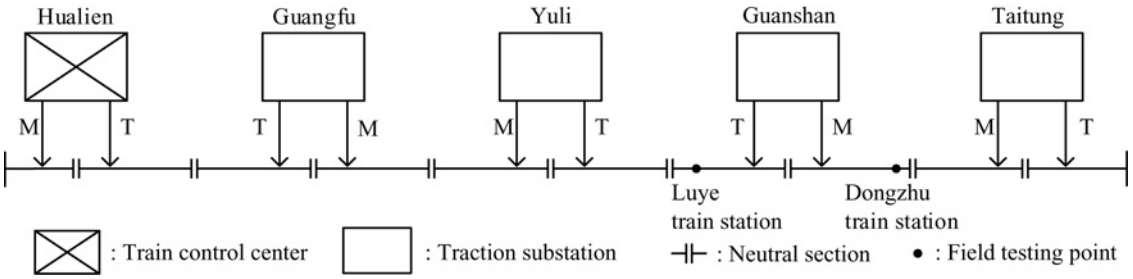

Fig. 1 *Arrangement of traction substations in Eastern Taiwan railway electrification system*

short-circuit analysis program based on a bus (node) admittance matrix. This makes it possible to derive the fault currents in each branch of a RTS as well as the profiles of fault currents along the route of the railway. It also enables the calculation of voltages in overhead messenger wires, overhead trolley contact wires, and return feeders along the route of the railway.

2 Railway electrification system

The railway electrification system in Eastern Taiwan includes five traction substations and four disconnecting switches, as shown in Fig. 1. A remote operation control centre situated in Hualien is used to supervise and control moving trains and the entire RTS. The power-supply zone for each traction substation is approximately 40 km, each of which is further separated into two power-supply sub-zones fed single-phase power from phases M and T of a Le Blanc transformer in traction substations. This necessitates the inclusion of a neutral zone to isolate out-of-phase electric power from phases M and T of the Le Blanc transformers.

Traction substations are usually located in the centre of a power-supply zone. Fig. 2 presents a single-line diagram of a traction substation typical of the Eastern Taiwan railway electrification system. As shown in Fig. 3, the traction substation transformer employs a special winding connection transformer (a Le Blanc transformer) to facilitate the balancing of system voltage. The primary windings used with the traction transformer are a delta connection fed by two 69 kV sub-transmission lines from discrete TPC bulk power substations. The secondary windings present a special Le Blanc connection, which provides two 25 kV electric power with 90° phase displacement for the moving trains. The traction substations are equipped with protective equipment, such as circuit breakers, disconnecting switches, and lightning arresters.

3 Mathematical model

The elements essential to a RTS include traction substations with traction transformers and OCS comprising overhead messenger wire, overhead trolley contact wire, return feeder, and rail. The modelling of system components is the key process dictating the success of system simulation. The precision of the simulation results as well as the convergence characteristics of solution techniques are determined by the system component models and full-scale network model. In this study, we employed a bus admittance matrix and coupling-free equivalent circuit for the development of the proposed models.

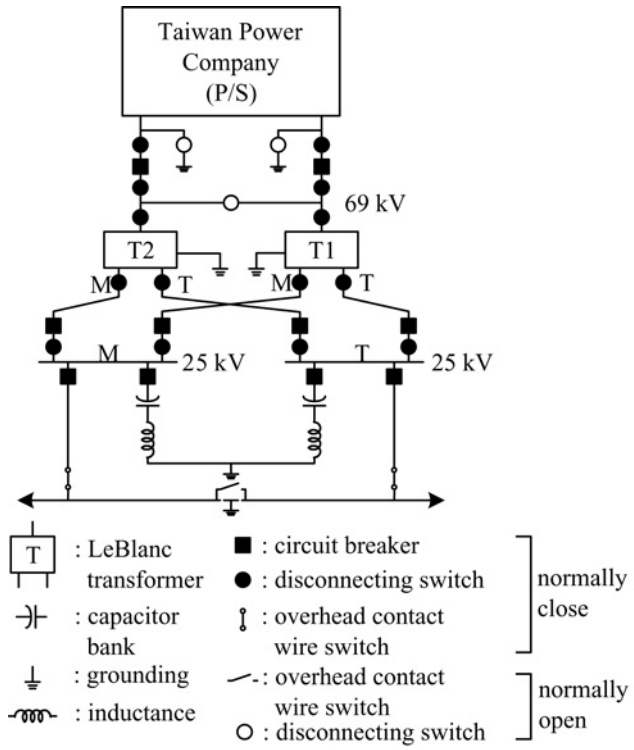

Fig. 2 *Single-line diagram of typical traction substation in Eastern Taiwan railway electrification system*

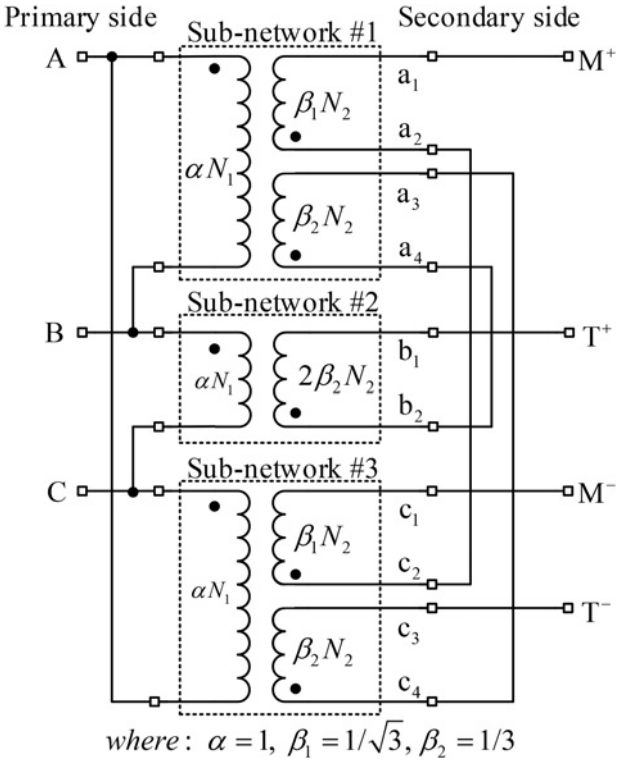

Fig. 3 *Le Blanc traction transformer connected using three single-phase transformers with delta-connected primary windings*

3.1 Le Blanc traction transformer

In the Eastern Taiwan railway electrification system, a special winding connection transformer (a Le Blanc transformer) is used in traction substations to alleviate system voltage imbalance caused by large single-phase traction loads. This approach is generally preferred over a Scott connection in railway electrification system, due to a common core with three-limb, three-phase design is employed for the construction of a Le Blanc transformer compared with two single-phase cores for the Scott transformer. In addition to a somewhat simpler standard core arrangement, the Le Blanc transformer is less costly to manufacture because for a given rating, less active materials are required for its construction [20]. Fig. 3 illustrates the winding connection of a Le Blanc transformer, in which the primary windings are in delta connection.

The mathematical model of a Le Blanc transformer can be derived as follows:

(i) The Le Blanc transformer with delta-connected primary windings is portioned into three sub-networks (i.e. sub-networks #1, #2, and #3) as shown in Fig. 3. The mathematical models of the three sub-networks (i.e. three single-phase transformers) can be obtained using the algorithms described in [21]. According to the structure of the single-phase transformers, the corresponding bus admittance matrix can be, respectively, represented using (1)–(3), where y_t represents the per unit leakage admittance of the single-phase transformers, obtained in a short-circuit test.

$$Y^{\#1} = \begin{array}{c} \\ \mathrm{A} \\ \mathrm{B} \\ \mathrm{a_1} \\ \mathrm{a_2} \\ \mathrm{a_3} \\ \mathrm{a_4} \end{array} \begin{array}{c} \begin{array}{cccccc} \mathrm{A} & \mathrm{B} & \mathrm{a_1} & \mathrm{a_2} & \mathrm{a_3} & \mathrm{a_4} \end{array} \\ \begin{bmatrix} 2 & -2 & -\beta_1^{-1} & \beta_1^{-1} & -\beta_2^{-1} & \beta_2^{-1} \\ -2 & 2 & \beta_1^{-1} & -\beta_1^{-1} & \beta_2^{-1} & -\beta_2^{-1} \\ -\beta_1^{-1} & \beta_1^{-1} & \beta_1^{-2} & -\beta_1^{-2} & 0 & 0 \\ \beta_1^{-1} & -\beta_1^{-1} & -\beta_1^{-2} & \beta_1^{-2} & 0 & 0 \\ -\beta_2^{-1} & \beta_2^{-1} & 0 & 0 & \beta_2^{-2} & -\beta_2^{-2} \\ \beta_2^{-1} & -\beta_2^{-1} & 0 & 0 & -\beta_2^{-2} & \beta_2^{-2} \end{bmatrix} \end{array} \times y_t \tag{1}$$

$$Y^{\#2} = \begin{array}{c} \\ \mathrm{B} \\ \mathrm{C} \\ \mathrm{b_1} \\ \mathrm{b_2} \end{array} \begin{array}{c} \begin{array}{cccc} \mathrm{B} & \mathrm{C} & \mathrm{b_1} & \mathrm{b_2} \end{array} \\ \begin{bmatrix} 1 & -1 & -(2\beta_2)^{-1} & (2\beta_2)^{-1} \\ -1 & 1 & (2\beta_2)^{-1} & -(2\beta_2)^{-1} \\ -(2\beta_2)^{-1} & (2\beta_2)^{-1} & (2\beta_2)^{-2} & -(2\beta_2)^{-2} \\ (2\beta_2)^{-1} & -(2\beta_2)^{-1} & -(2\beta_2)^{-2} & (2\beta_2)^{-2} \end{bmatrix} \end{array} \times y_t \tag{2}$$

$$Y^{\#3} = \begin{array}{c} \\ \mathrm{C} \\ \mathrm{A} \\ \mathrm{c_1} \\ \mathrm{c_2} \\ \mathrm{c_3} \\ \mathrm{c_4} \end{array} \begin{array}{c} \begin{array}{cccccc} \mathrm{C} & \mathrm{A} & \mathrm{c_1} & \mathrm{c_2} & \mathrm{c_3} & \mathrm{c_4} \end{array} \\ \begin{bmatrix} 2 & -2 & -\beta_1^{-1} & \beta_1^{-1} & -\beta_2^{-1} & \beta_2^{-1} \\ -2 & 2 & \beta_1^{-1} & -\beta_1^{-1} & \beta_2^{-1} & -\beta_2^{-1} \\ -\beta_1^{-1} & \beta_1^{-1} & \beta_1^{-2} & -\beta_1^{-2} & 0 & 0 \\ \beta_1^{-1} & -\beta_1^{-1} & -\beta_1^{-2} & \beta_1^{-2} & 0 & 0 \\ -\beta_2^{-1} & \beta_2^{-1} & 0 & 0 & \beta_2^{-2} & -\beta_2^{-2} \\ \beta_2^{-1} & -\beta_2^{-1} & 0 & 0 & -\beta_2^{-2} & \beta_2^{-2} \end{bmatrix} \end{array} \times y_t \tag{3}$$

(ii) The bus admittance matrix of a Le Blanc transformer with delta-connected primary windings can then be obtained by combining the bus admittance matrices of the three single-phase transformers. In addition, the internal nodes (i.e. a_3, a_4, b_2, c_2, and c_4) can be removed using Kron's law, as shown in (4). Following the same procedure, we can obtain a model of the Le Blanc transformer with wye-connected primary windings, as shown in (5).

$$Y^{\Delta}_{\mathrm{LeBlanc}} = Y^{\#1} + Y^{\#2} + Y^{\#3}$$

$$= \begin{array}{c} \\ \mathrm{A} \\ \mathrm{B} \\ \mathrm{C} \\ \mathrm{M^+} \\ \mathrm{M^-} \\ \mathrm{T^+} \\ \mathrm{T^-} \end{array} \begin{array}{c} \begin{array}{ccccccc} \mathrm{A} & \mathrm{B} & \mathrm{C} & \mathrm{M^+} & \mathrm{M^-} & \mathrm{T^+} & \mathrm{T^-} \end{array} \\ \begin{bmatrix} 2y_1 & -y_1 & -y_1 & 2y_2 & -2y_2 & 0 & 0 \\ -y_1 & 2y_1 & -y_1 & -y_2 & y_2 & y_3 & -y_3 \\ -y_1 & -y_1 & 2y_1 & -y_2 & y_2 & -y_3 & y_3 \\ 2y_2 & -y_2 & -y_2 & y_3 & -y_3 & 0 & 0 \\ -2y_2 & y_2 & y_2 & -y_3 & y_3 & 0 & 0 \\ 0 & y_3 & -y_3 & 0 & 0 & y_3 & -y_3 \\ 0 & -y_3 & y_3 & 0 & 0 & -y_3 & y_3 \end{bmatrix} \end{array} \tag{4}$$

$$Y^{\mathrm{Y}}_{\mathrm{LeBlanc}} = \begin{array}{c} \\ \mathrm{A} \\ \mathrm{B} \\ \mathrm{C} \\ \mathrm{M^+} \\ \mathrm{M^+} \\ \mathrm{T^+} \\ \mathrm{T^-} \end{array} \begin{array}{c} \begin{array}{ccccccc} \mathrm{A} & \mathrm{B} & \mathrm{C} & \mathrm{M^+} & \mathrm{M^-} & \mathrm{T^+} & \mathrm{T^-} \end{array} \\ \begin{bmatrix} -\frac{2}{3}y_1 & -\frac{1}{3}y_1 & -\frac{1}{3}y_1 & y_2 & -y_2 & -\frac{1}{3}y_3 & \frac{1}{3}y_3 \\ -\frac{1}{3}y_1 & -\frac{2}{3}y_1 & -\frac{1}{3}y_1 & 0 & 0 & \frac{2}{3}y_2 & -\frac{2}{3}y_2 \\ -\frac{1}{3}y_1 & -\frac{1}{3}y_1 & -\frac{2}{3}y_1 & -y_2 & y_2 & -\frac{1}{3}y_3 & \frac{1}{3}y_3 \\ y_2 & 0 & -y_2 & y_3 & -y_3 & 0 & 0 \\ -y_2 & 0 & y_2 & -y_3 & y_3 & 0 & 0 \\ -\frac{1}{3}y_3 & \frac{2}{3}y_2 & -\frac{1}{3}y_3 & 0 & 0 & y_3 & -y_3 \\ \frac{1}{3}y_3 & -\frac{2}{3}y_2 & \frac{1}{3}y_3 & 0 & 0 & -y_3 & y_3 \end{bmatrix} \end{array} \tag{5}$$

where

$$y_1 = \frac{3-\sqrt{3}}{2}y_t,\ y_2 = \frac{3(\sqrt{3}-1)}{4}y_t,\ y_3 = \frac{3(3-\sqrt{3})}{4}y_t$$

(iii) According to (4) and (5), the corresponding coupling-free equivalent circuits of the Le Blanc transformer are presented in

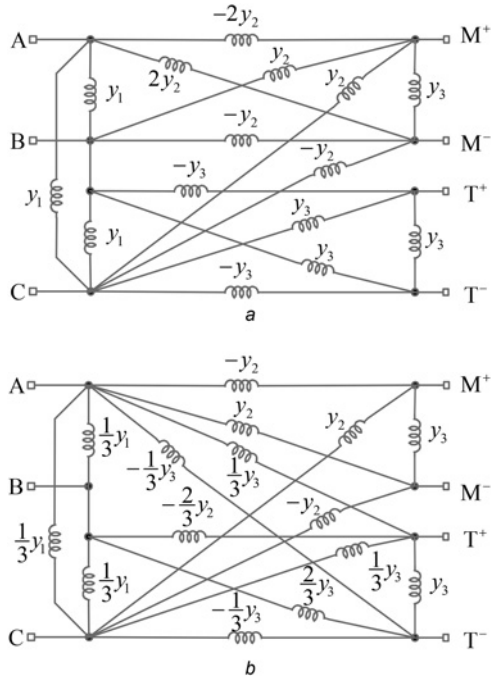

Fig. 4 *Coupling-free equivalent circuit of Le Blanc transformer*
a Delta-connected primary windings
b wye-connected primary windings

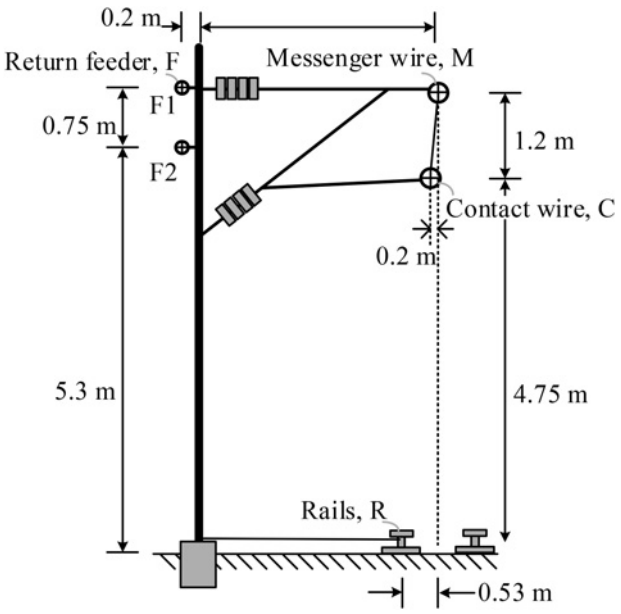

Fig. 5 *Geometric structure of AC railway traction pole used in Eastern Taiwan railway electrification system*

Fig. 4*a* (with delta-connected primary windings) and Fig. 4*b* (with wye-connected primary windings).

3.2 Overhead catenary system

Depending on traffic density, a railway electrification system may consist of one, two, three, or four tracks. The OCS for Eastern Taiwan railway electrification system consists of overhead messenger wire, overhead contact wire, rails, return feeder 1 and return feeder 2, as shown in Fig. 5, in which the overhead contact system includes an overhead messenger wire, overhead trolley contact wire and two return feeders. The circuit used for the return of traction power to traction substations includes running rails and return feeders.

The mathematical model of OCS was derived as follows:

(i) In general, an OCS has inherent geometrical asymmetrical structure and unbalanced current carried in different lines; therefore, its detailed model should consider the arrangement of the overhead contact lines, taking into account the spacing between overhead lines and running rails, and the physical position for each individual overhead line. Carson proposed a method to determine the self and mutual impedances for overhead multi-conductor circuits considering the effect of the earth [22]. Further, the equations derived by Carson can be applied to underground cables and railway OCSs. Carson used

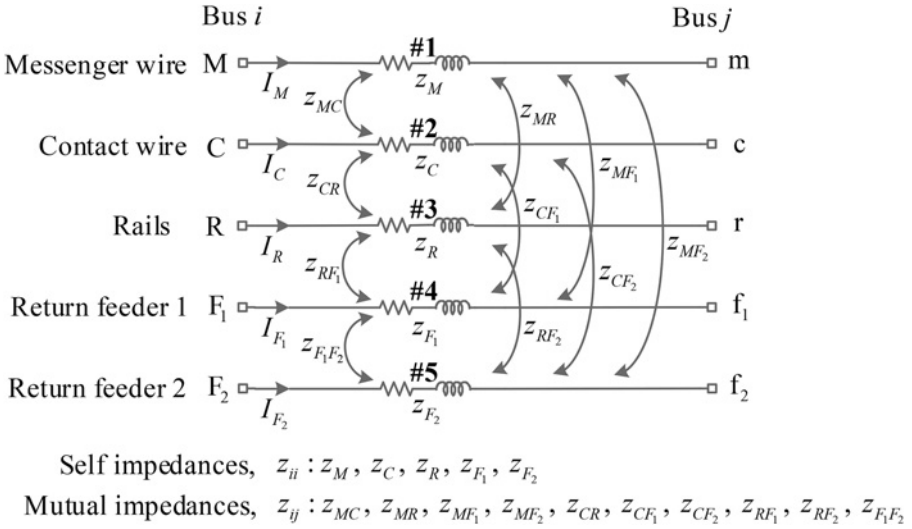

Fig. 6 *Schematic representation of self and mutual impedances of OCS in the Eastern Taiwan railway electrification system*

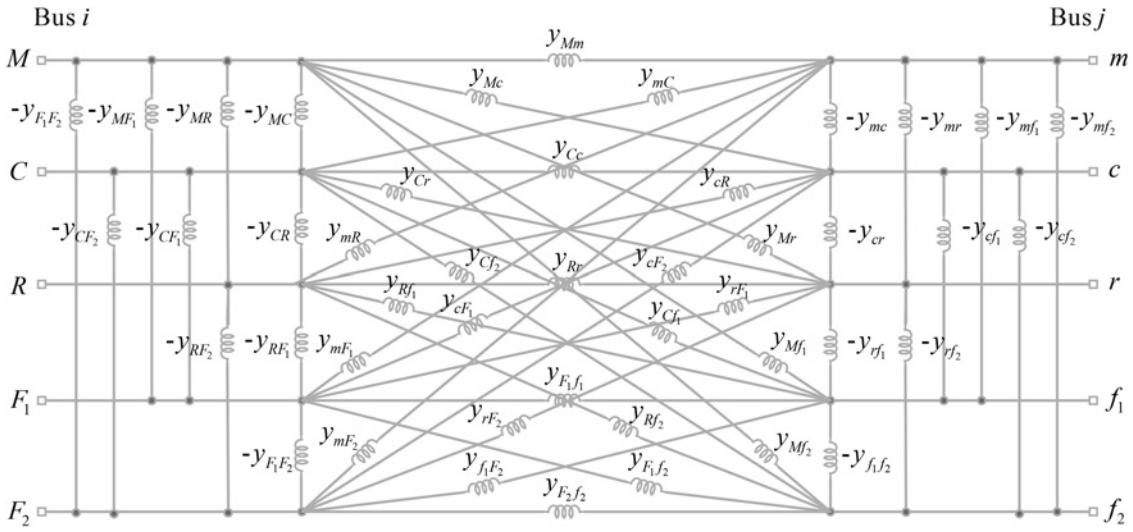

Fig. 7 *Coupling-free equivalent circuit of an OCS*

the method of images based on the assumption that the earth an equipotential plane, and therefore, the electric flux lines are forced to cut the surface of the earth orthogonally. Hence, the earth effect can be represented by placing an oppositely charged conductor (image conductor) below the surface of the earth by a distance equal to that of the overhead conductor above the earth for all conductors in the OCS. Carson's original equations are given in [22]. Because Carson's original equations are somewhat complex, some approximations are made to simplify their calculations. In [23], Carson's modified equations are developed, and these equations are applied for calculating the primitive self and mutual impedances of the overhead lines in an OCS in this study. It was assumed that: (i) the frequency of the railway electrification system is 60 Hz, and (ii) the earth resistivity is 100 Ω-metre. A set of modified Carson's equations are given in (6) and (7).

$$\hat{z}_{ii} = r_i + 0.09327 + j0.12134\left(\ln\left(\frac{1}{\mathrm{GMR}_i}\right) + 7.95153\right) \quad (6)$$

$$\hat{z}_{ij} = 0.09327 + j0.12134\left(\ln\left(\frac{1}{D_{ij}}\right) + 7.95153\right) \quad (7)$$

where $\hat{z}_{ii}$: self-impedance of conductor i in Ω/mile; $\hat{z}_{ij}$: mutual-impedance between conductors i and j in Ω/mile; r_i: resistance of conductor i in Ω/mile; GMR_i: geometric mean radius of conductors i in feet; and D_{ij}: distance between conductors i and j in feet.

(ii) Fig. 6 presents an equivalent schematic circuit of an OCS including running rails. All overhead lines are modelled as a π model. However, all shunt capacitances of the overhead lines are disregarded because the power-supply zones of phases T and M of the traction transformer from traction substations are quite short, usually less than 20 km.

The primitive equations that relate the node voltages and branch currents of overhead lines in an OCS are shown in a compact form as

$$\begin{bmatrix} V_{\mathrm{M}} \\ V_{\mathrm{C}} \\ V_{\mathrm{R}} \\ V_{\mathrm{F}_1} \\ V_{\mathrm{F}_2} \end{bmatrix} = \begin{bmatrix} V_m \\ V_c \\ V_r \\ V_{f_1} \\ V_{f_2} \end{bmatrix} + l \times \begin{bmatrix} z_{\mathrm{M}} & z_{\mathrm{MC}} & z_{\mathrm{MR}} & z_{\mathrm{MF}_1} & z_{\mathrm{MF}_2} \\ z_{\mathrm{MC}} & z_{\mathrm{C}} & z_{\mathrm{CR}} & z_{\mathrm{CF}_1} & z_{\mathrm{CF}_2} \\ z_{\mathrm{MR}} & z_{\mathrm{CR}} & z_{\mathrm{R}} & z_{\mathrm{RF}_1} & z_{\mathrm{RF}_2} \\ z_{\mathrm{MF}_1} & z_{\mathrm{CF}_1} & z_{\mathrm{RF}_1} & z_{\mathrm{F}_1} & z_{\mathrm{F}_1\mathrm{F}_2} \\ z_{\mathrm{MF}_2} & z_{\mathrm{CF}_2} & z_{\mathrm{RF}_2} & z_{\mathrm{F}_1\mathrm{F}_2} & z_{\mathrm{F}_2} \end{bmatrix} \times \begin{bmatrix} I_{\mathrm{M}} \\ I_{\mathrm{C}} \\ I_{\mathrm{R}} \\ I_{\mathrm{F}_1} \\ I_{\mathrm{F}_2} \end{bmatrix} \quad (8)$$

where l is the overhead line length of an OCS. Further, (6) and (7) are used to find the self and mutual impedances, respectively. The corresponding primitive impedance matrix $[\boldsymbol{z}_{\mathrm{pr}}]$ that considers the self and mutual impedances of the overhead messenger wire, overhead contact wire, running rails, and two return feeders are given as

$$[\boldsymbol{z}_{\mathrm{pr}}] = \begin{bmatrix} z_{\mathrm{M}} & z_{\mathrm{MC}} & z_{\mathrm{MR}} & z_{\mathrm{MF}_1} & z_{\mathrm{MF}_2} \\ z_{\mathrm{MC}} & z_{\mathrm{C}} & z_{\mathrm{CR}} & z_{\mathrm{CF}_1} & z_{\mathrm{CF}_2} \\ z_{\mathrm{MR}} & z_{\mathrm{CR}} & z_{\mathrm{R}} & z_{\mathrm{RF}_1} & z_{\mathrm{RF}_2} \\ z_{\mathrm{MF}_1} & z_{\mathrm{CF}_1} & z_{\mathrm{RF}_1} & z_{\mathrm{F}_1} & z_{\mathrm{F}_1\mathrm{F}_2} \\ z_{\mathrm{MF}_2} & z_{\mathrm{CF}_2} & z_{\mathrm{RF}_2} & z_{\mathrm{F}_1\mathrm{F}_2} & z_{\mathrm{F}_2} \end{bmatrix} \quad (9)$$

(iii) The branch-bus incident matrix $\boldsymbol{C}$ for Fig. 6 is as follows

$$\boldsymbol{C} = \begin{array}{c} \\ \#1 \\ \#2 \\ \text{brach}\#3 \\ \#4 \\ \#5 \end{array} \begin{array}{c} \begin{array}{ccccccccccc} & \multicolumn{5}{c}{\text{bus } i} & & \multicolumn{5}{c}{\text{bus } j} \\ & \mathrm{M} & \mathrm{C} & \mathrm{R} & \mathrm{F}_1 & \mathrm{F}_2 & m & c & r & f_1 & f_2 \end{array} \\ \begin{bmatrix} 1 & 0 & 0 & 0 & 0 & -1 & 0 & 0 & 0 & 0 \\ 0 & 1 & 0 & 0 & 0 & 0 & -1 & 0 & 0 & 0 \\ 0 & 0 & 1 & 0 & 0 & 0 & 0 & -1 & 0 & 0 \\ 0 & 0 & 0 & 1 & 0 & 0 & 0 & 0 & -1 & 0 \\ 0 & 0 & 0 & 0 & 1 & 0 & 0 & 0 & 0 & -1 \end{bmatrix} \end{array} \quad (10)$$

(iv) Using (9) and (10), the bus admittance matrix of railway OCS was obtained as (11). (see (11))

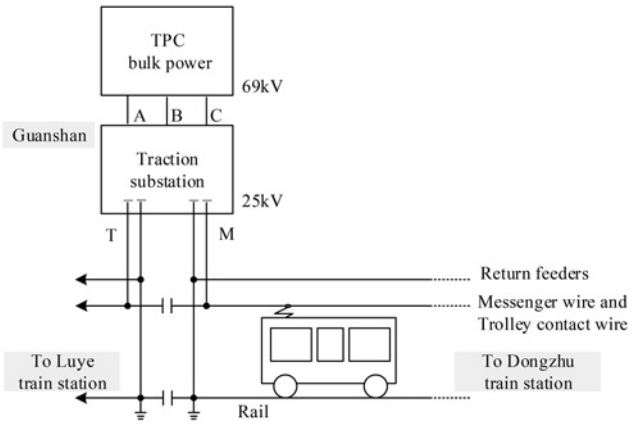

Fig. 8 *One-line diagram of the Eastern Taiwan railway electrification system at Guanshan traction substation*

$$\boldsymbol{Y}_{\mathrm{RES}} = C^t\left[\boldsymbol{z}_{\mathrm{pr}}\right]^{-1}\boldsymbol{C} = \begin{bmatrix} y_{\mathrm{M}} & y_{\mathrm{MC}} & y_{\mathrm{MR}} & y_{\mathrm{MF}_1} & y_{\mathrm{MF}_2} & -y_{Mm} & -y_{Mc} & -y_{Mr} & -y_{Mf_1} & -y_{Mf_2} \\ y_{\mathrm{MC}} & y_{\mathrm{C}} & y_{CR} & y_{\mathrm{CF}_1} & y_{\mathrm{CF}_2} & -y_{Cm} & -y_{Cc} & -y_{Cr} & -y_{Cf_1} & -y_{Cf_2} \\ y_{\mathrm{MR}} & y_{\mathrm{CR}} & y_{\mathrm{R}} & y_{\mathrm{RF}_1} & y_{\mathrm{RF}_2} & -y_{Rm} & -y_{Rc} & -y_{Rr} & -y_{Rf_1} & -y_{Rf_2} \\ y_{\mathrm{MF}_1} & y_{\mathrm{CF}_1} & y_{\mathrm{RF}_1} & y_{\mathrm{F}_1} & y_{\mathrm{F}_1\mathrm{F}_2} & -y_{F_1m} & -y_{F_1c} & -y_{F_1r} & -y_{F_1f_1} & -y_{F_1f_2} \\ y_{\mathrm{MF}_2} & y_{\mathrm{CF}_2} & y_{\mathrm{RF}_2} & y_{\mathrm{F}_1\mathrm{F}_2} & y_{\mathrm{F}_2} & -y_{F_2m} & -y_{F_2c} & -y_{F_2r} & -y_{F_2f_1} & -y_{F_2f_2} \\ -y_{Mm} & -y_{Cm} & -y_{Rm} & -y_{F_1m} & -y_{F_2m} & y_m & y_{mc} & y_{mr} & y_{mf_1} & y_{mf_2} \\ -y_{Mc} & -y_{Cc} & -y_{Rc} & -y_{F_1c} & -y_{F_2c} & y_{mc} & y_c & y_{cr} & y_{cf_1} & y_{cf_2} \\ -y_{Mr} & -y_{Cr} & -y_{Rr} & -y_{F_1r} & -y_{F_2r} & y_{mr} & y_{cr} & y_r & y_{rf_1} & y_{rf_2} \\ -y_{Mf_1} & -y_{Cf_1} & -y_{Rf_1} & -y_{F_1f_1} & -y_{F_2f_1} & y_{mf_1} & y_{cf_1} & y_{rf_1} & y_{f_1} & y_{f_1f_2} \\ -y_{Mf_2} & -y_{Cf_2} & -y_{Rf_2} & -y_{F_1f_2} & -y_{F_2f_2} & y_{mf_2} & y_{cf_2} & y_{rf_2} & y_{f_1f_2} & y_{f_2} \end{bmatrix} \quad (11)$$

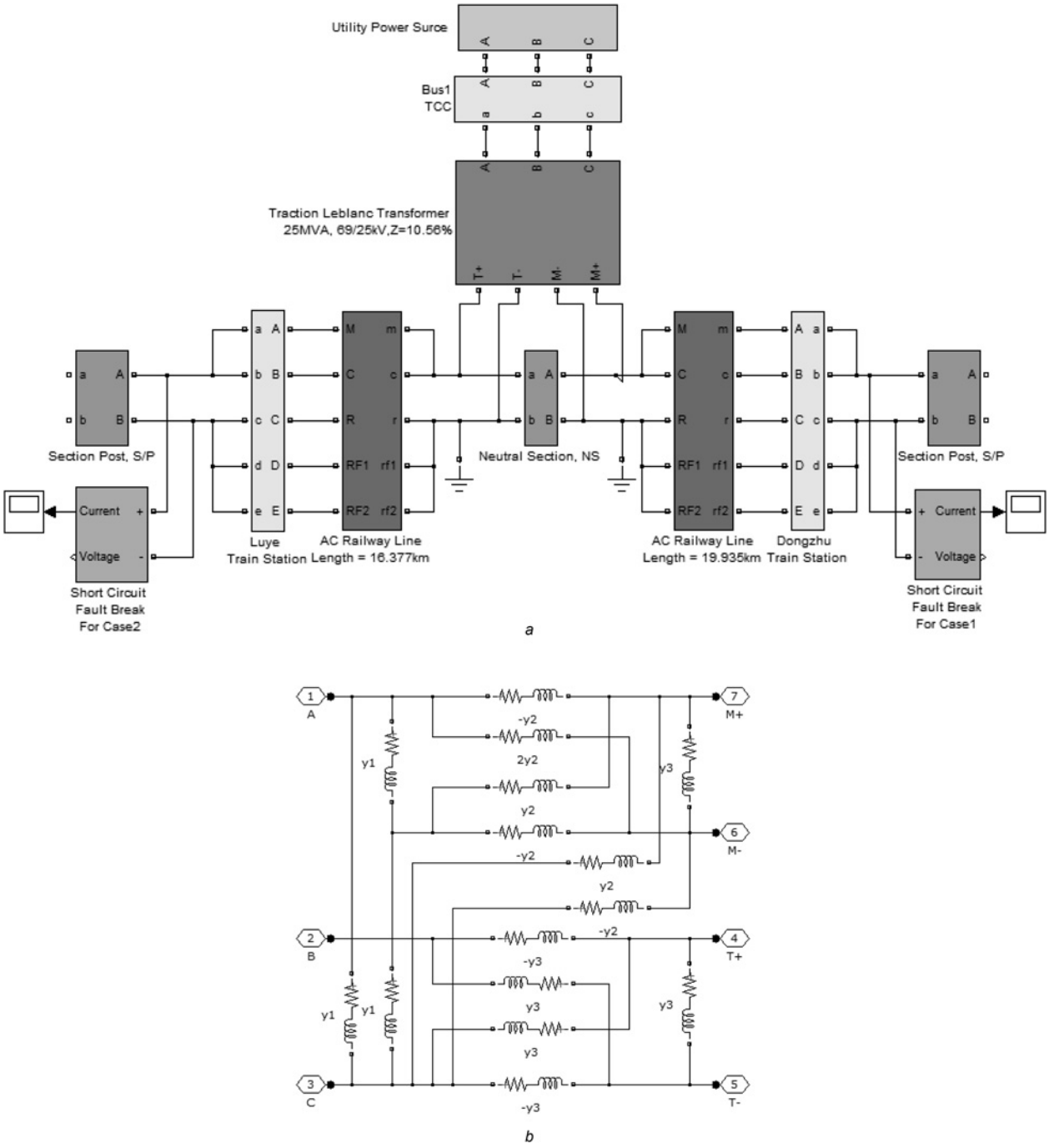

Fig. 9 *Block diagrams created using MATLAB®/Simulink®*

a Full-scale model of the Eastern Taiwan railway electrification system at a typical traction substation area
b Coupling-free equivalent circuit of a Le Blanc traction transformer
c Coupling-free equivalent circuit of an OCS

(v) According to (11), the corresponding coupling-free equivalent circuit of the OCS is shown in Fig. 7.

3.3 Utility power source

The impedance of the power-supply source should be taken into account for fault analysis because of its sizable effect on the fault current. The equivalent impedance of the source can be obtained by converting the SCC on the source side of the traction transformer. In this paper, the circuit model of a utility power sources is represented by a Thevenin's equivalent circuit [24].

4 Implementation procedure

Short-circuit field testing in a high-voltage network can be highly dangerous and time-consuming; therefore, only limited testing cases are subsidised. In contrast, a precise component model and a full-scale RTS model can be used to obtain nearly the same results as those obtained from the testing field. An appropriate computer program not only helps engineers select, design, and operate a RTS, but also provides a useful tool for determining the correct

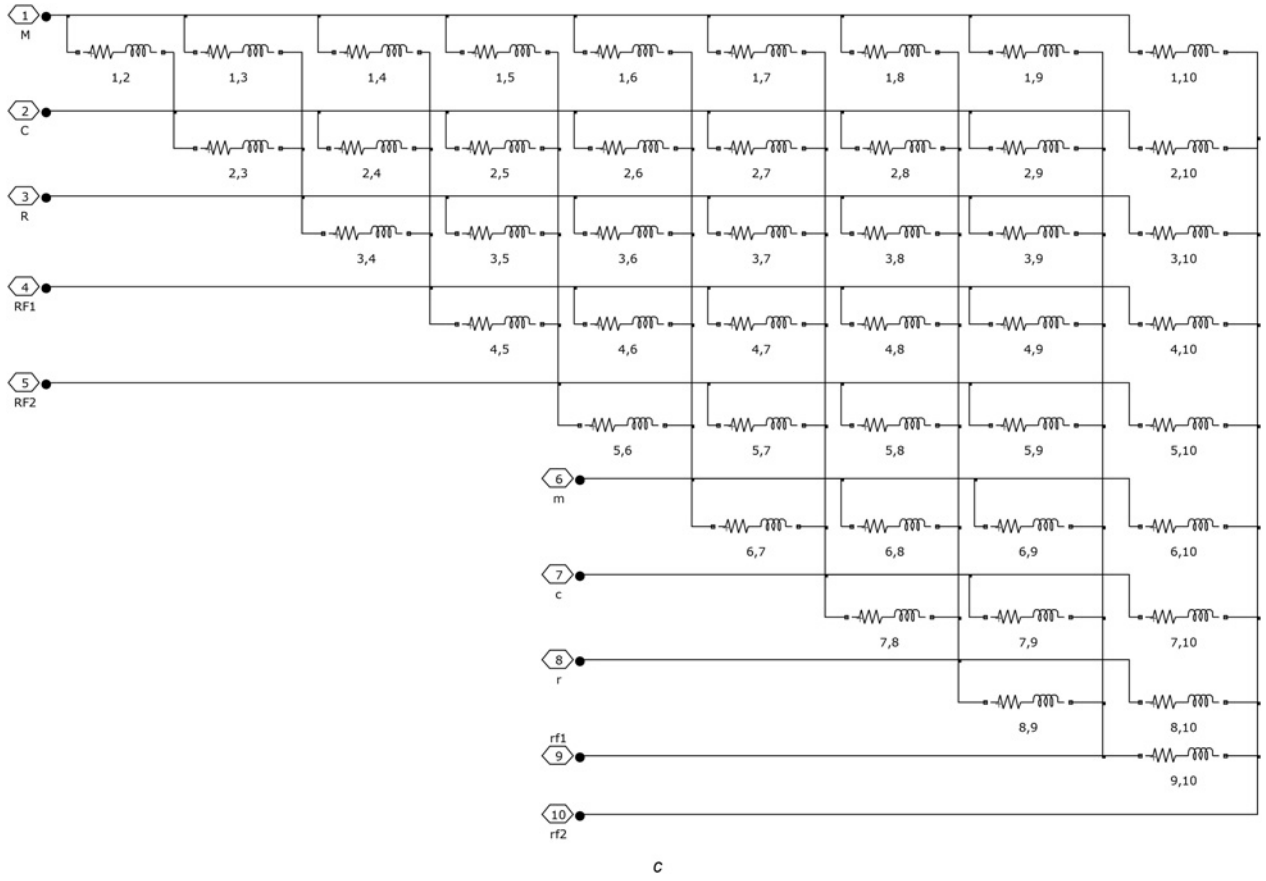

Fig. 9 *(Continued).*

short-circuit currents for various fault scenarios. A commercial simulation software package called MATLAB®/Simulink®, which has powerful simulation ability and a user-friendly graphical interface, was adopted to simulate the RTS of the Eastern Taiwan railway electrification system. All major components need to be properly modelled by their corresponding equivalent circuits before the RTS can be simulated using MATLAB®/Simulink®. The Le Blanc traction transformer and OCS can be represented explicitly in the MATLAB®/Simulink®. Hence, the OCS can be analysed in more detail. The steps for modelling the RTS of the Eastern Taiwan railway electrification system are as follows:

(i) *Forming equivalent circuit models for all major components in the target RTS* In MATLAB®/Simulink®, the coupling-free equivalent circuits can be represented by simple elements such as resistance, inductance, capacitance, and voltage/current sources, that is, coupling-free equivalent circuits can be modified and modularised to meet the requirements of different simulation objectives, and then be implemented with MATLAB®/Simulink®. Modularisation is useful for MATLAB®/Simulink® functions where users can construct their own component models and full-scale system models.

(ii) *Setting necessary parameters for all system components* Unsuitable or incorrect parameters may result in incorrect simulation results and confusing conclusions, and may lead to program divergence. All required parameters of the major components in the target RTS must be collected.

(iii) *Building a full-scale model of the target RTS* According to the structure of the target RTS, a full-scale system model can be built by combining the major component models, such as Le Blanc traction transformer and OCS.

The one-line diagram of the Eastern Taiwan railway electrification system at Guanshan substation is shown in Fig. 8 and its corresponding full-scale network model implemented using MATLAB®/Simulink® is illustrated in Fig. 9*a*. The branches and nodes of the major components, such as the Le Blanc traction transformer and OCS are explicitly represented as shown in Figs. 9*b*–*c*.

5 Field testing and simulation results

5.1 Field testing

A short-circuit fault was field tested within the power-supply zone of the Guanshan traction substation [25]. A solid short-circuit fault was introduced between the overhead contact line and the running rail.

Table 1 Parameters of the overhead contact line and running rail of the target OCS

Measuring point	Measurement data					Calculated data			
	AC voltage, V	AC current, A	cos θ	Active power, P (kW)	Reactive power, Q (kvar)	Resistance, R (Ω)	Reactance, X (Ω)	Impedance, Z (Ω)	Angle, θ
Dongzhu	305.40	33.97	0.2554	2.64	10.03	2.29	8.69	8.990	75.2
Luye	305.40	41.30	0.2870	3.62	12.07	2.05	7.10	7.394	73.9

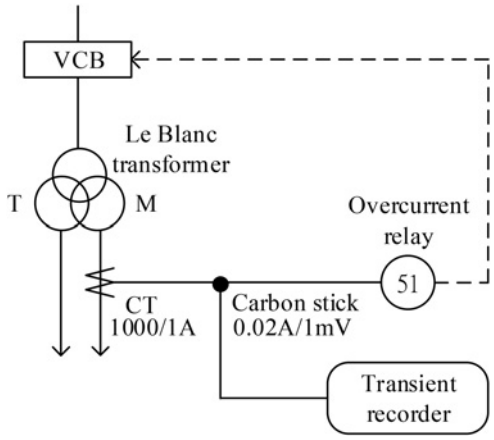

Fig. 10 *Schematic connection diagram for short-circuit current measurement*

To reveal the variations in the short-circuit current along the power-supply zone, the ends of the power-supply zone – phases M and T of the transformer from the Guanshan traction substation – were selected as fault points that are located at the Dongzhu (Case 1) and Luye (Case 2) train stations, respectively (see Fig. 1).

The short-circuit fault testing procedure is as follows:

(i) Ensure that there is no train in the power-supply zone and the OCS is de-energised and temporarily grounded so that there is no residual voltage on the target overhead contact lines.

(ii) Short-circuit the overhead contact line and the rail at the fault points, that are located at the Dongzhu (Case 1) and Luye (Case 2) train stations.

(iii) Measure the parameters of the target overhead contact lines and calculate their corresponding impedance and resistance. The overhead contact line system is a complicated system; the magnitude, phase angle of voltage and current, and the active and reactive powers are measured while a proper current is injected between the overhead contact line and the rail at the traction substation. Next, the equivalent impedance of the overhead contact line and running rail of the target power-supply zone is calculated. Table 1 summarises the measured and calculated results. This table indicates that the system equivalent resistance at the Luye train station is less compared with that at the Dongzhu's train station.

(iv) Using the calculated data in Table 1, along with the given traction transformer impedance and system equivalent impedance at the primary side of the traction transformer, calculate the short-circuit current before the real short-circuit is performed. The calculated fault currents were applied to the settings of the fault current recording instruments so that the waveform of the short-circuit current can be exactly recorded, and unnecessary repetitive tests can be avoided.

(v) Reenergise the target overhead contact line before the short-circuit test are conducted. More functions of the related relay and vacuum circuit breaker (VCB) should be endorsed.

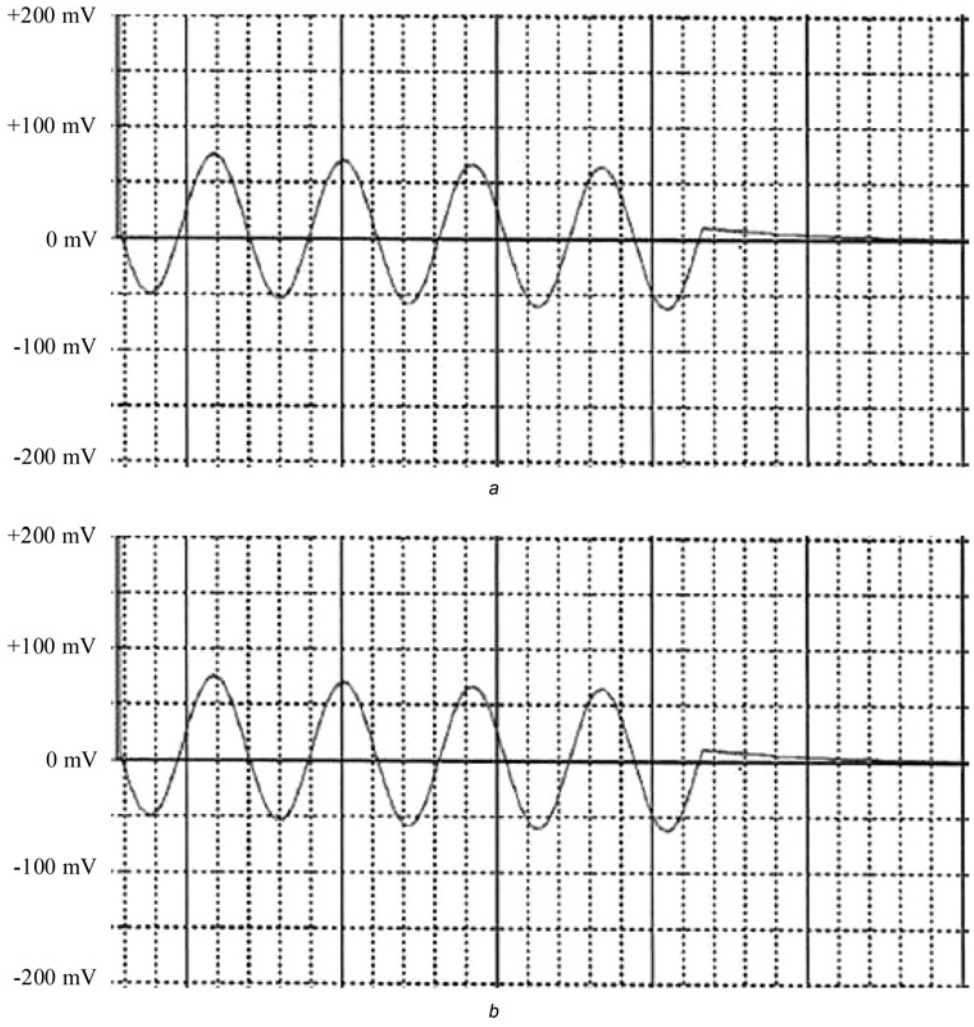

Fig. 11 *Field testing result of short-circuit fault*

a ($I_{SC\text{-}case1}$) at Dongzhu train station
b ($I_{SC\text{-}case2}$) at Luye train station

Table 2 Parameters used in railway electrification system

Conductors	Resistance, Ω/mile	GMR, ft.	*X*, m	*Y*, m
messenger wire	0.19490	7.2033	3.15	5.95
contact wire	0.16355	12.000	2.95	4.75
rails	0.04076	45.160	2.62	0.00
return feeder 1	0.27210	9.5557	−0.20	6.05
return feeder 2	0.27210	9.5557	−0.20	5.30

(vi) Perform short-circuit tests, record the transient fault currents, and analyse the fault current waveform for comparison with simulation results.

The short-circuit test at high voltage system is not only dangerous but also highly expensive. The equipment, overhead contact line circuit, and all the connections should be checked in detail visually and using instrument inspection equipment before the short-circuit test can be carried out. In addition, the testing procedure should be strictly followed to ensure safety. Moreover, the route of the overhead catenary line system should be guarded, especially at railway crossings. All personnel on duty at fault points, measuring locations, traction substations, and railway crossings, should keep close contact using telephones or mobile phones. These requirements confirm that the short-circuit test is undoubtedly time-consuming and expensive. Therefore, in this study, only two of these tests were completed owing to time and cost constraints.

To measure the fault current waveform during the short-circuit test, the current-to-voltage carbon stick was used to convert the output current of the current transformer (CT) to voltage signals. The CT was installed on the secondary side of the Le Blanc traction transformer; therefore, the transient fault current could be recorded using this transient recorder. Fig. 10 illustrates the connection for short-circuit current measurement wherein the overcurrent relay (51) with automatic action capability is automatically triggered to interrupt the VCB to isolate the faulted zone if a short-circuit fault occurs.

The transient recorders record the current waveform when a short-circuit fault occurred, whereupon a VCB caused an interruption after approximately four cycles as shown in Fig. 11. Fig. 11*a* presents the results of field testing of a short-circuit fault on the phase M at Dongzhu train station. Fig. 11*b* presents the results of field testing of a short-circuit fault on the phase T, at Luye train station.

In most cases, short-circuit current would include components of symmetric AC current as well as asymmetrical DC. The asymmetrical DC component of the fault current lasts only a few cycles, as shown in Figs. 11*a* and *b*. However, the asymmetrical DC component of the fault current mainly depends on momentary voltage, system *X*/*R* ratio, and the timing of the short-circuit fault. Thus, the maximum direct short-circuit current was difficult to obtain by controlling the voltage injection time.

Furthermore, the field testing results in Figs. 11*a* and *b* provide a valuable reference for use in verifying the precision of simulation results. For example, each peak value of the measured fault current waveform can be used to calculate the time constant and X/R of the fault point, whereas the recorded amplitude is used to calculate the AC fault current. All of the fault currents are in root mean square (rms) values; therefore, momentary fault current can be obtained by multiplying the recorded peak voltage value (representing the short-circuit fault current) by the turn ratio

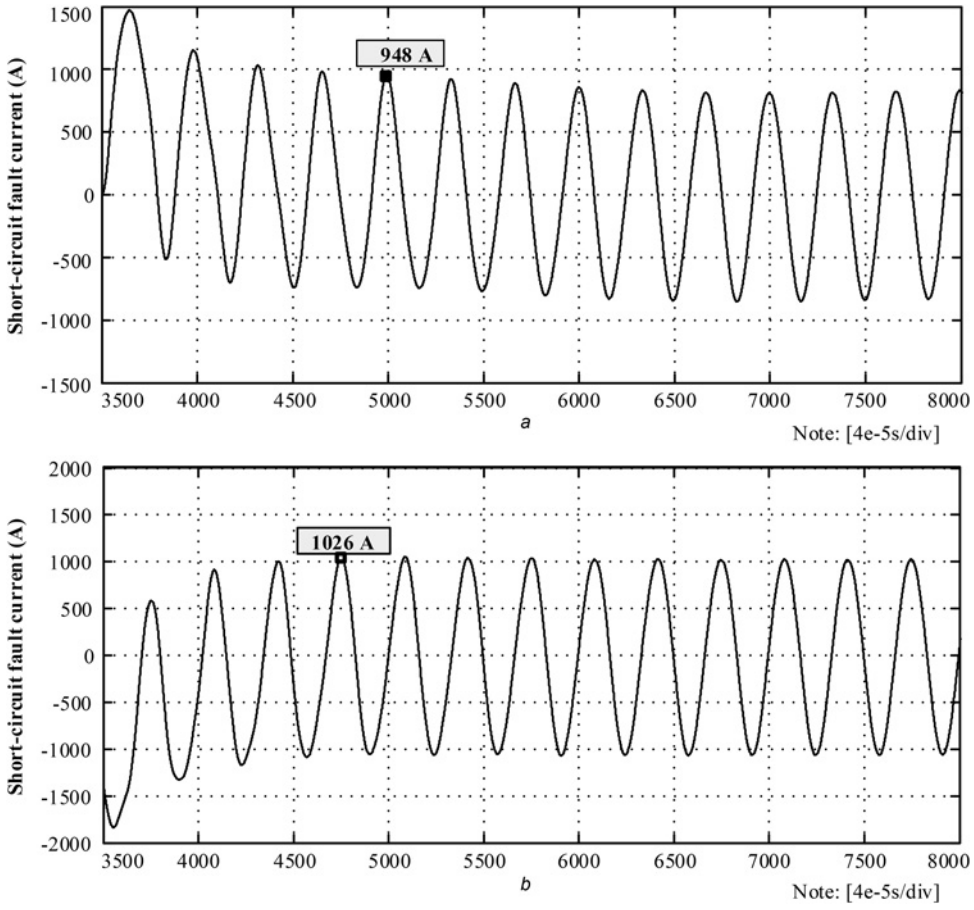

Fig. 12 *Simulation results of short-circuit fault*

a ($I_{SC\text{-}case1}$) at Dongzhu train station
b ($I_{SC\text{-}case2}$) at Luye train station

settings of the carbon stick and CT, which is then divided . On the basis of the short-circuit fault current waveform shown in Figs. 11*a* and *b*, their corresponding actual rms short-circuit fault currents can be calculated is as following:

(i) $I_{SC\text{-}case1}$ = (50 mV/DIV) × (1.33 DIV) × (0.707) × (0.02 A/1 mV) × (1000/1 A) = 940.45 A, for fault at Dongzhu train station.
(ii) $I_{SC\text{-}case2}$ = (50 mV/DIV) × (1.48 DIV) × (0.707) × (0.02 A/1 mV) × (1000/1 A) = 1046 A, for fault at Luye train station.

5.2 Parameters

The parameters used in the simulation are listed as follows:

(i) The equivalent impedance of the utility power source is calculated according to a SCC of 364.5 MVA and rated voltage of 69 kV, as provided by the TPC. This voltage source was considered ideal and the phase-to-phase voltages are specified.
(ii) The parameters used in the Le Blanc traction transformer are as follows: primary windings in delta connection, rated capacity 25 MVA, 69/25 kV, the leakage impedance of 10.56%.
(iii) The distance between two railway poles is 50 m. The distance between Dongzhu train station and Guanshan substation is 19.935 km. The distance between Luye train station and Guanshan substation is 16.377 km.

Table 3 Comparison of short-circuit rms currents obtained through field testing and simulation

Field testing point	Fault distance from substation, km	Fault rms current, A	
		Field testing	Simulation
Dongzhu	19.935	940.5	948
Luye	16.377	1046	1026

(iv) Ground resistivity was assumed to be 100 Ω-m. The railway poles are grounded with multiple grounding branches used to prevent harmonic current flowing through the rail from interfering with nearby communication lines.
(v) The parameters used for the AC railway line (see Fig. 5) of the Eastern Taiwan of railway electrification system are listed in Table 2 using a Cartesian coordinate system [26].

5.3 Simulation

Short-circuit faults were simulated using the full-scale model of the railway electrification system established in the previous section. Simulation enabled the control of the phase angle of the pre-fault voltage. Figs. 12*a* and *b* presents the simulation results of short-circuit current waveforms. As shown in Table 3, a comparison of results from computer simulation and field testing

Table 4 Short-circuit currents and voltages under various fault conditions

System operating model	R_{SC}, Ω	*d*, km	Branch current, A					Voltage, kV
			I_{SC}	I_M	I_C	I_R	I_F	V_{Tr}
Tr.#1: on Tr.#2: off	0	20	963.7∠97.9°	443.8∠98.3°	519.9∠97.6°	520.6∠−87.1°	447.4∠−76.3°	11.98
		18	1011.7∠97.5°	465.9∠97.9°	545.8∠97.2°	546.5∠−87.5°	469.7∠−76.6°	11.31
		16	1064.7∠97.1°	490.3∠97.5°	574.4∠96.8°	575.1∠−87.9°	494.3∠−77.1°	10.58
		12	1188.9∠96.1°	547.5∠96.5°	641.4∠95.8°	642.2∠−88.9°	552.0∠−78.1°	8.864
		8	1345.4∠94.8°	619.6∠95.2°	725.8∠94.5°	726.8∠−90.2°	624.6∠−79.4°	6.687
		4	1548.1∠93.1°	712.9∠93.5°	835.2∠92.8°	836.3∠−91.9°	718.7∠−81.1°	3.847
		2	1673.5∠92.1°	770.7∠92.5°	902.9∠91.8°	904.0∠−92.9°	776.9∠−82.1°	2.080
	1	20	955.2∠101.0°	439.9∠101.4°	515.3∠100.7°	516.0∠−84.0°	443.4∠−73.2°	12.30
		18	1002.6∠100.8°	461.7∠101.2°	540.9∠100.4°	541.6∠−84.2°	465.5∠−73.4°	11.68
		16	1055.0∠100.5°	485.8∠100.9°	569.1∠100.2°	569.9∠−84.5°	489.8∠−73.7°	10.99
		12	1177.9∠99.9°	542.5∠100.3°	635.5∠99.6°	636.3∠−85.1°	546.8∠−74.3°	9.372
		8	1333.1∠99.1°	613.9∠99.5°	719.2∠98.8°	720.1∠−85.9°	618.9∠−75.1°	7.365
		4	1534.9∠98.1°	706.9∠98.5°	828.1∠97.8°	829.2∠−86.9°	712.6∠−76.1°	4.874
		2	1660.4∠97.5°	764.6∠97.9°	895.8∠97.1°	896.9∠−87.5°	770.8∠−76.7°	3.521
	5	20	898.9∠112.5°	413.9∠112.9°	484.9∠112.2°	485.6∠−72.5°	417.3∠−61.7°	14.27
		18	940.6∠112.8°	433.2∠113.2°	507.4∠112.5°	508.1∠−72.2°	436.7∠−61.4°	13.89
		16	986.3∠113.2°	454.2∠113.6°	532.1∠112.8°	532.8∠−71.8°	457.9∠−61.0°	13.49
		12	1092.4∠114.0°	503.1∠114.4°	589.4∠113.6°	590.1∠−71.0°	507.2∠−60.2°	12.65
		8	1223.8∠115.0°	563.6∠115.4°	660.2∠114.6°	661.1∠−70.0°	568.2∠−59.2°	11.85
		4	1390.5∠116.3°	640.3∠116.7°	750.2∠115.9°	751.1∠−68.7°	645.5∠−57.9°	11.27
		2	1491.7∠117.0°	687.0∠117.4°	804.8∠116.7°	805.8∠−68.0°	692.5∠−57.2°	11.19
Tr.#1: on Tr.#2: on	0	20	1037.9∠98.3°	478.0∠98.7°	560.0∠98.0°	560.7∠−86.7°	481.8∠−75.9°	12.89
		18	1093.9∠97.9°	503.8∠98.3°	590.2∠97.6°	590.9∠−87.1°	507.8∠−76.3°	12.23
		16	1156.1∠97.4°	532.4∠97.9°	623.7∠97.1°	623.7∠−87.6°	536.7∠−76.7°	11.49
		12	1304.2∠96.4°	600.6∠96.8°	703.6∠96.0°	704.5∠−88.6°	605.5∠−77.8°	9.724
		8	1495.1∠95.0°	688.5∠95.4°	806.6∠94.6°	807.6∠−90.0°	694.1∠−79.2°	7.431
		4	1749.8∠93.1°	805.8∠93.5°	944.0∠92.8°	945.2∠−91.9°	812.4∠−81.1°	4.349
		2	1911.7∠91.9°	880.4∠92.3°	1031.4∠91.6°	1032.7∠−93.1°	887.5∠−82.3°	2.376
	1	20	1027.5∠101.6°	473.2∠102.0°	554.4∠101.3°	555.1∠−83.4°	477.0∠−72.6°	13.24
		18	1082.7∠101.4°	498.6∠101.8°	584.1∠101.0°	584.8∠−83.6°	502.6∠−72.8°	12.61
		16	1144.0∠101.1°	526.9∠101.5°	617.2∠100.8°	618.0∠−83.9°	531.1∠−73.1°	11.91
		12	1290.2∠100.5°	594.2∠100.9°	696.1∠100.2°	697.0∠−84.5°	599.0∠−43.7°	10.27
		8	1479.0∠99.8°	681.1∠100.4°	797.9∠99.4°	799.0∠−85.2°	686.7∠−74.4°	8.171
		4	1732.1∠98.7°	797.7∠99.1°	934.5∠98.4°	935.7∠−86.3°	804.1∠−75.4°	5.500
		2	1893.8∠98.1°	872.1∠98.5°	1021.7∠97.7°	1023.0∠−86.9°	879.2∠−76.1°	4.016
	5	20	959.2∠113.9°	441.7∠114.3°	517.5∠113.5°	518.2∠−71.1°	445.3∠−60.3°	15.23
		18	1006.7∠114.3°	463.6∠114.7°	543.1∠113.9°	543.8∠−70.7°	467.4∠−59.9°	14.86
		16	1059.1∠114.7°	487.7∠115.1°	571.4∠114.4°	572.1∠−70.3°	491.7∠−59.5°	14.48
		12	1181.8∠115.8°	544.2∠116.2°	637.6∠115.4°	638.4∠−69.2°	548.7∠−58.4°	13.69
		8	1336.0∠117.1°	615.3∠117.5°	720.8∠116.8°	721.7∠−67.9°	620.3∠−57.1°	12.94
		4	1535.4∠118.8°	707.1∠119.2°	828.3∠118.5°	829.4∠−66.2°	712.8∠−55.4°	12.45
		2	1658.4∠119.9°	763.7∠120.3°	894.7∠119.6°	895.8∠−65.1°	769.9∠−54.3°	12.44

Notes: The variables are described as follows; d: distance of fault location away from traction substation; R_{SC}: fault resistance; I_{SC}: short-circuit fault current; I_M: fault current in overhead messenger wire; I_C: fault current in overhead contact wire; I_F: the sum of fault currents in the two return feeders; and V_{Tr}: voltage at the traction station outgoing busbar

revealed a difference of between 0.79% and 1.91%. The factors contributing to this variation are as follows:

(i) Visual error: This is the primary source of error due to the fact that even slight visual errors can be magnified when a short-circuit fault of up to 1000 A appears on the screen of the transient recorder.
(ii) Instrumentation error: The instruments used for testing are likely to introduce measurement error.
(iii) The validity of the components and full-scale models, the technical solutions that are selected, and the assumptions made for the simulation can all exert a profound effect on the results.

Table 3 confirms that the proposed models can precisely retrieve the characteristics of a 1×25 kV railway electrification system for short-circuit analysis. In addition, the proposed models and solution approach can be used to make more detailed simulations, and therefore, can detect the features and limitations of the target system that cannot be done by only the field tests. The following detailed short-circuit analysis results were obtained by the proposed approach.

(i) For the short-circuit fault occurred at Dongzhu train station (Case 1), the detailed steady-state short-circuit currents flowing through the individual contact lines in the OCS are identified as follows: $I_{\text{SC-case1}} = I_{\text{M}} + I_{\text{C}} = -(I_{\text{R}} + I_{\text{F}}) = 965.21\angle 97.92°$ A, $I_{\text{M}} = 444.5\angle 98.32°$ A, $I_{\text{C}} = 520.73\angle 97.57°$ A, $I_{\text{R}} = 521.4\angle -87.08°$ A, and $I_{\text{F}} = I_{\text{F1}} + I_{\text{F2}} = 448.1\angle -76.26°$ A (the sum of the currents flowing in the two return feeders). The steady-state voltage of the traction station outgoing busbar can also be identified, that is $11.96\angle 172.18°$ kV with a voltage deviation of 52.2%.
(ii) For the short-circuit fault that occurred at the Luye train station (Case 2), the detailed steady-state short-circuit currents flowing through the individual contact lines in the OCS are as follows: $I_{\text{SC-case2}} = 1054.28\angle 7.19°$ A, $I_{\text{M}} = 485.52\angle 7.60°$ A, $I_{\text{C}} = 568.78\angle 6.85°$ A, $I_{\text{R}} = 569.51\angle -177.87°$ A, and $I_{\text{F}} = 489.45\angle -166.99°$ A. The steady-state voltage of traction station outlet end is $10.73\angle 81.45°$ kV with a voltage deviation of 57.08%.

Moreover, two fault impedances (0, 1, and 5 Ω), seven fault locations (2, 4, 8, 12, 16, 18, and 20 km from traction substation) and two system operating conditions (Tr #1: on, Tr #2: off; Tr #1: on, Tr #2: on) were simulated for considering the effect of fault impedance, fault location, and system configuration on the fault currents and voltages. The simulation results are summarised in Table 4. The short-circuit currents provide significant information for the selection of protective relays and circuit breakers. Accordingly, the proposed approach provides a valuable reference for power engineers involved in the planning, design, and operation of a railway traction network.

6 Conclusions

This study developed mathematical models of the major components as well as a full-scale representation of a 1×25 kV railway electrification system for analysis of short-circuits. The proposed models of a Le Blanc transformer and a RTS are represented using their corresponding coupling-free equivalent circuits and implemented using the commercial software package, MATLAB®/Simulink®. The models developed in this paper could be applied to the simulation of short-circuit faults occurring in any location of a railway electrification system as a means of avoiding the dangers and costs associated with field testing.

The Eastern Taiwan railway electrification system was introduced and used as a demonstration system for short-circuit analysis. The full-scale model of the demonstration system was created by combining the equivalent circuit models for its major components such as the Le Blanc traction transformer model and the OCS model. The coupling-free equivalent circuit of the full-scale model was implemented using MATLAB®/Simulink®. Next, a series of digital simulations were performed for various short-circuit conditions. Finally, the simulation and field test results was compared. The comparison indicated that the proposed models can precisely retrieve the characteristics of a 1×25 kV railway electrification system for short-circuit analysis. Based on the above facts, the proposed models and solution approach could provide a valuable reference for power engineers involved in the planning, design, and operation of a railway traction network.

In addition, the proposed models and solution approach can be used to perform more simulations, and therefore, help detect the features and limitations of the target system that cannot be done only through field tests. At present, the proposed models are being used to optimise and upgrade the Taiwan railway's electrification system. Future works will aim at power flow study, harmonic analysis, voltage drop calculation, substation grounding system analysis, and protective relay coordination study.

7 Acknowledgment

The author thank the CECI Engineering Consultants, Inc., Taiwan for providing the measurement data.

8 References

1 Courtois, C.: 'Why the 2 × 25 kV alternative? [autotransformer traction supply]'. IEE Colloquium on 50 kV Autotransformer Traction Supply System – the French Experience, November 1993, pp. 1–4
2 Roussel, H.: 'Power supply for the Atlantic TGV high speed line'. Int. Conf. on Main Line Railway Electrification, Set. 1989, pp. 388–392
3 Millard, A., Taylor, I.A., Weller, G.C.: 'AC electrified railways – protection and distance to fault measurement'. Int. Conf. on Electric Railways in United Europe, March 1995, pp. 73–77
4 Bailey, D.I., Jones, K.M.: 'The supply of large rail traction loads from small isolated power systems', IET Conference Publication No. 210, *Sources Eff. Power Syst. Disturb.*, 1982, pp. 260–266
5 Ross, B.A.: 'Meeting tomorrow's railroad power requirements', *IEEE Trans. Power Appar. Syst.*, 1971, **PAS-90**, (2), pp. 393–400
6 Hill, R.J., Brillante, S., Leonard, P.J.: 'Railway track transmission line parameters from finite element field modelling: series impedance', *IEE Proc. – Electr. Power Appl.*, 1999, **146**, (6), pp. 647–660
7 Hill, R.J., Brillante, S., Leonard, P.J.: 'Railway track transmission line parameters from finite element field modelling: shunt admittance', *IEE Proc. – Electr. Power Appl.*, 2000, **147**, (3), pp. 227–238
8 Mingli, W., Chengshan, X., Fan, Y., *et al.*: 'Performance and mathematical model of three-phase three-winding transformer used in 2 × 25 kV electric railway', *IEE Proc. – Electr. Power Appl.*, 2006, **153**, (2), pp. 271–281
9 Mariscotti, A., Pozzobon, P.: 'Determination of the electrical parameters of railway traction lines: calculation, measurements, and reference data', *IEEE Trans. Power Deliv.*, 2004, **19**, (4), pp. 1538–1546
10 Mariscotti, A., Pozzobon, P.: 'Resistence and internal inductance of traction rails at power frequency: a survey', *IEEE Trans. Veh. Technol.*, 2004, **53**, (4), pp. 1069–1075
11 Kneschke, T.A., Hong, J., Natarajan, R., *et al.*: 'Impedance calculations for SEPTA's rail power distribution system'. Proc. 1995 IEEE/ASME Joint Railroad Conf., April 1995, pp. 79–85
12 Natarajan, R., Kneschke, T.A., Naqvi, W., *et al.*: 'Short circuit currents of the SEPTA traction power distribution system', *IEEE Ind. Appl. Mag.*, 1997, **3**, (6), pp. 52–59
13 Cella, R., Giangaspero, G., Mariscotti, A., *et al.*: 'Measurements of AT electric railway system currents at power supply frequency and validation of a multiconductor transmission line model', *IEEE Trans. Power Deliv.*, 2006, **21**, (3), pp. 1721–1726
14 Chen, T.H., Hsu, Y.F.: 'Systematized short-circuit analysis of a 2 × 25 kV electric traction network', *Electr. Power Syst. Res.*, 1998, **47**, (2), pp. 133–142
15 Battistelli, L., Pagano, M., Proto, D.: 'Short circuit modelling and simulation of 2 × 25 kV high speed railways'. 2008. AICMS 08. Second Asia Int. Conf. on Modelling and Simulation, May 2008, pp. 702–707
16 Battistelli, L., Pagano, M., Proto, D.: '2 × 25-kV 50 Hz high-speed traction power system: short-circuit modeling', *IEEE Trans. Power Deliv.*, 2011, **26**, (3), pp. 1459–1466
17 Amendola, A., Battistelli, L., Candurro, L., *et al.*: 'Steady state and transient short circuit analysis of 2 × 25 kV high speed railways'. Proc. 8th World Congress on Railway Research, May 2008
18 Lee, H., Lee, C., Jang, G., *et al.*: 'Harmonic analysis of the korean high-speed railway using the eight-port representation model', *IEEE Trans. Power Deliv.*, 2006, **21**, (2), pp. 979–986
19 Mariscotti, A., Pozzobon, P., Vanti, M.: 'Simplified modelling of a 2 × 25-kV AT railway system for the solution of a low frequency and large-scale problems', *IEEE Trans. Power Deliv.*, 2007, **22**, (1), pp. 296–301
20 Stigant, S.A., Franklin, A.C.: 'The J & P transformer book: a practical technology of the power transformer' (London, Boston, 1973), pp. 150–205

21 Chen, T.H., Huang, M.Y.: 'Network modelling of 24-pulse rectifier transformers for rigorous simulation of rail transit power systems', *Electr. Power Syst. Res.*, 1999, **50**, (1), pp. 23–33
22 Carson, J.R.: 'Wave propagation in overhead wires with ground return', *Bell Syst. Tech. J.*, 1926, **5**, (4), pp. 539–554
23 Kersting, W.H., Green, R.K.: 'The application of Carson's equation to the steady-state analysis of distribution feeders'. Power Systems Conf. and Exposition, March 2011, pp. 1–6
24 Chen, T.H., Kuo, H.Y.: 'Network modelling of traction substation transformers for studying unbalance effects', *IEE Proc.-Gener. Transm. Distrib.*, 1995, **142**, (2), pp. 103–108
25 Tatung Company: 'East railway improvement project – power supply system: static test report' (Railway Reconstruction Bureau Ministry of Transportation and Communications, 2011), pp. 221–224
26 Chang, S.H.: 'Analysis of voltage unbalance in the electric railway depot using two-port network model', *Korean Inst. Electr. Eng.*, 2001, **50**, pp. 248–256